6. G. C. Pomraning, *The Equations of Radiation Hydrodynamics* (Pergamon Press, NY, 1973).

7. M. Born and E. Wolf, *Principles of Optics*, 5th ed. (Pergamon Press, Oxford, 1975), p. 122.

8. A. Yariv, *Quantum Electronics*, 2nd ed. (Wiley, New York, 1975), p. 285.

9. M. D. Rosen *et al.*, *Phys. Rev. Lett.* **59**, 2283 (1987).

10. D. Shvarts, B. Yaakobi, P. Audebert, T. Boehly, B. Boswell, D. Bradley, R. S. Craxton, R. Epstein, M. C. Richardson, and J. M. Soures, *X Rays from Laser Plasmas* (SPIE, Bellingham, WA, 1987), Vol. 831, pp. 283–292.

2.B Time-Resolved Spectroscopic Measurements of High Density in Ar-Filled Microballoon Implosions

In current high-density, laser-driven implosion experiments the determination of core conditions at stagnation is of great importance. This is particularly true of fusion experiments (D_2- or DT-filled targets) where nuclear diagnostics have been developed to estimate final core conditions.[1,2] A complementary approach, relying on x-ray spectroscopy of high-Z gases (as total fill gas or as dopant), provides values of the electron density and temperature.[3–6] This technique has the added advantage that, with the inclusion of x-ray streak-camera technology, these parameters can be followed in time during the implosion. In addition to providing a valuable fusion diagnostic, this approach offers the opportunity to study the spectroscopy of many different highly stripped ions under extremely high-density conditions. In this article, we report time-resolved spectroscopic analysis of compressed, high-Z gas-filled targets.

In a series of experiments supported by the NLUF, C. F. Hooper, D. P. Kilcrease, R. C. Mancini, and L. A. Woltz of the University of Florida, in collaboration with laboratory scientists, studied the implosion of Ar-filled plastic microballoons of dimensions 420 μm × 6 μm (diameter × wall thickness).[7] These experiments used the 24-beam, UV (λ = 0.35 μm) OMEGA laser system, operated with the maximum illumination uniformity afforded by new distributed-phase-plate technology.[8] The total incident laser energy was 1700 J within a Gaussian pulse of duration 680±50 ps (FWHM). The targets were filled to pressures of 2 or 10 atm of Ar. A broad array of diagnostics,

including time-resolved, x-ray line spectroscopy with the SPEAXS curved crystal streak spectrograph[9] and time-integrated x-ray imaging of the compressed core, was deployed. Figures 38.25 and 38.26 show spectra recorded on two shots for different target pressures. The x-ray energy range shown covers emission from the He_α and Ly_α transitions of He- and H-like Ar and their associated satellite structure. Emission from the He_β and Ly_β lines was too weak for spectroscopic analysis (higher members of the helium and Lyman series either were not seen or lie beyond the energy range covered by the spectrograph). Spectra recorded from the implosion of an empty target were used to determine the extent of instrument-generated structure in the

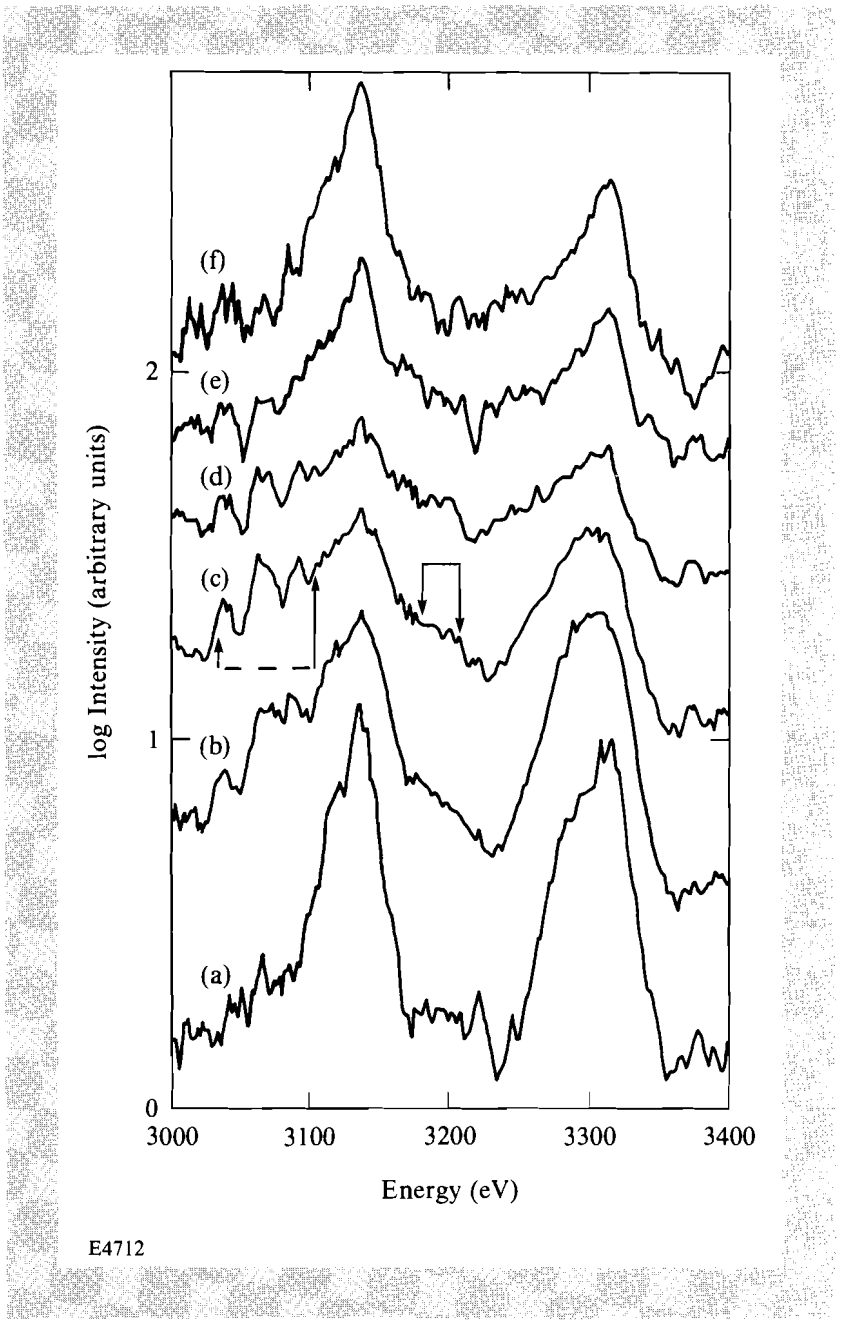

Fig. 38.25
Series of time-resolved spectra for the 2-atm case. Spectrums (c) and (d) correspond to implosion stagnation. (– – – –) inner-shell transitions in C-, B- and Be-like Ar; (→) broad "blue satellite" feature. These spectra have been shifted vertically by arbitrary amounts for the purpose of suitable display in the same picture.

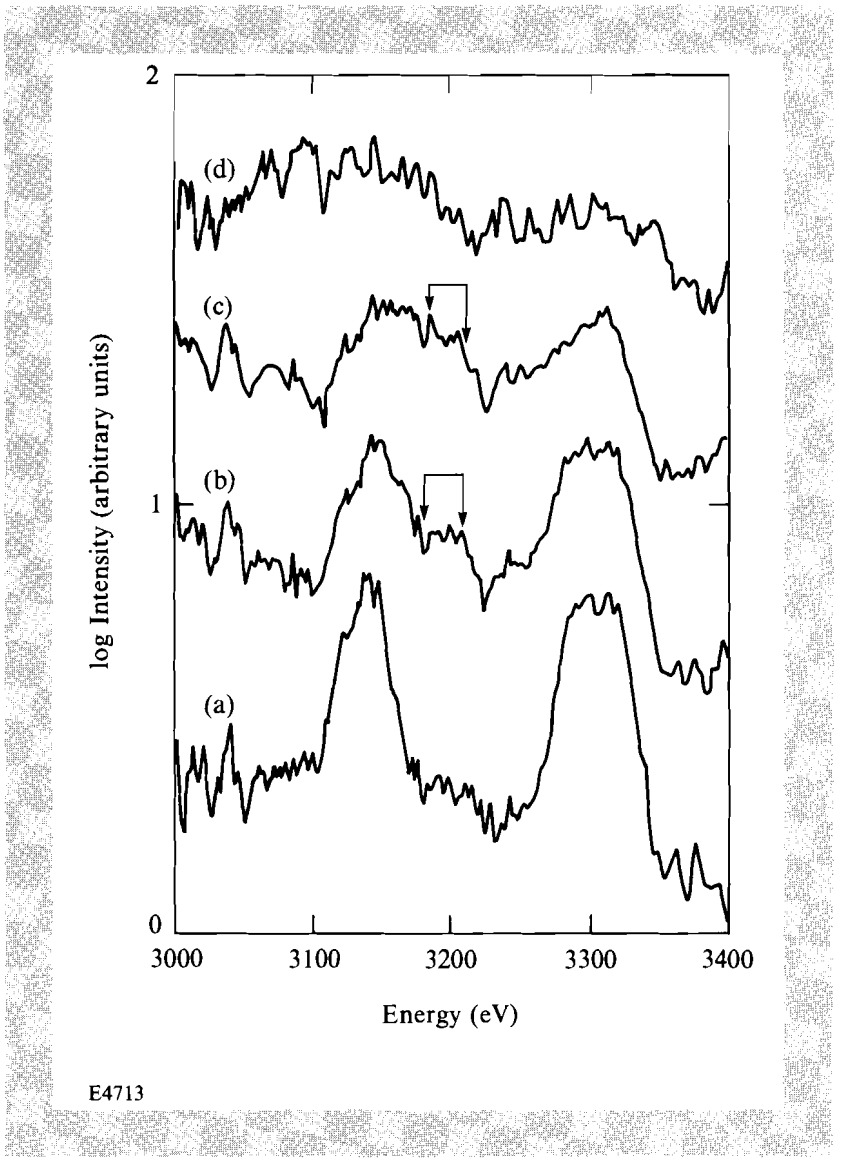

Fig. 38.26
Same as in Fig. 38.25, but for the 10-atm case. In this case, spectrum (c) is characteristic of the stagnation. Note that after the stagnation (d), only continuum emission is seen.

continuum background. Figures 38.25 and 38.26 show time sequences of spectra obtained during the implosion. The He-like satellites ($2\ell 2\ell'$-$1s2\ell$) of Ly_α are very intense and, together with the Ly_α line, give rise to the spectral feature located around 3300 eV, whose low-energy side is dominated by satellite transitions and high-energy side by the Ly_α line. Since the line shapes of the satellite and resonant transitions have been broadened sufficiently to cause merging, it is not possible to resolve the separate spectral features as was possible in previous implosion experiments.[10-12] As the implosion progresses, the overall shape of this composite spectral feature broadens further and shows varying degrees of asymmetry. While this line persists after the implosion for the low-pressure target (Fig. 38.25), only continuum emission is observed for the high-pressure target (Fig. 38.26). The spectral feature associated with the He_α line and its Li-like satellites also shows an interesting evolution; as time advances we see the onset of an unusual emission feature ($\sim$3160 eV to 3220 eV) on the blue or

high-energy wing of the He_α line in addition to the usual red satellites ($1s2\ell2\ell'$ - $1s^22\ell$) found on the low-energy wing. This feature is observed in both Fig. 38.25 and Fig. 38.26. These broadened blue satellites achieve their highest intensity at the time of stagnation, when the maximum density is reached. For the target with the lower fill pressure, these features disappear when the system begins to decompress. A similar qualitative behavior has been observed in time-resolved spectra from other high-density implosion experiments.[13] In Fig. 38.25 we notice, between 3040 and 3100 eV, three emission peaks corresponding to the inner-shell transitions in C-, B- and Be-like argon. The evolution of their intensity can be observed before and at the implosion's stagnation. In Fig. 38.26 we see the red wing of the He_α line partially truncated as the implosion approaches stagnation. We interpret this as an incipient absorption feature due to transitions in lower-ionization stages.

These spectra are compared to both Stark- and opacity-broadened theoretical line profiles to provide a history of the electron density and temperature during the implosion. The Stark-broadened line profiles, for different densities and temperatures, were computed for the Ly_α line of H-like Ar and its He-like satellite transitions using a recently developed multielectron line profile code.[14] In previous spectroscopic diagnosis, based on analysis of He-like satellites of the Ly_α line, the satellite line profile was approximated by a set of Lorentzian or Voigt

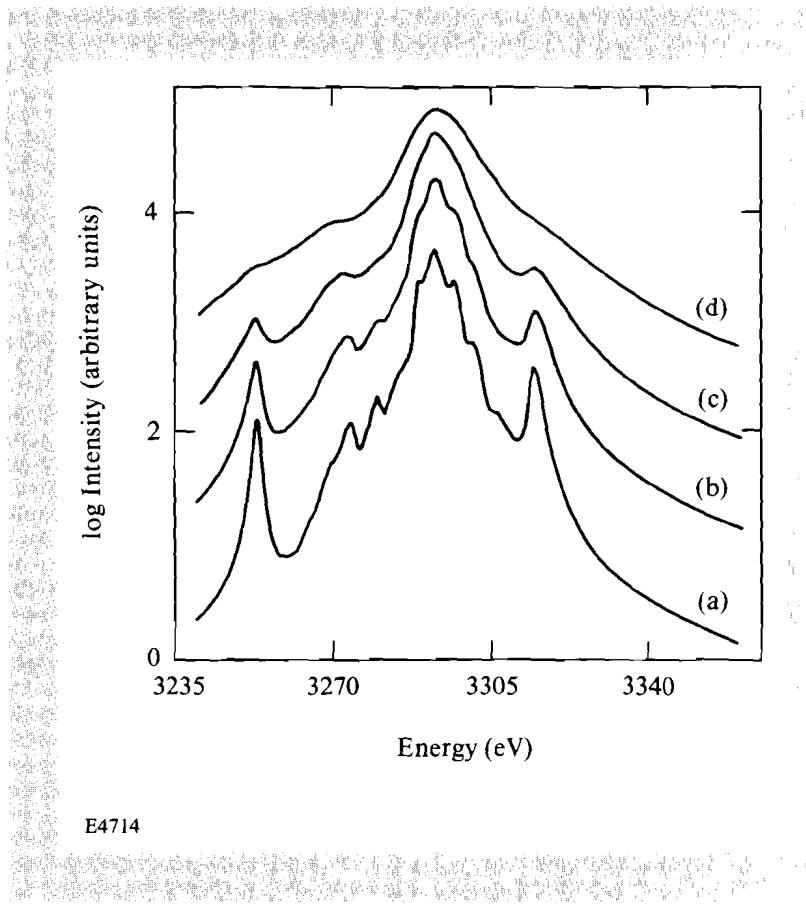

Fig. 38.27
He-like satellite line profiles for Ar^{+16} for an electron temperature T_e = 800 eV and densities of $N_e = 5 \times 10^{23}$ (a); 1×10^{24} (b); 2×10^{24} (c); and 5×10^{24} (d) in cm^{-3}.

line profiles whose individual widths were determined by instrumental broadening. However, we find that as the density increases, Stark-broadening and field-mixing effects become more important and can introduce substantial changes to the Voigt satellite line shapes. For example, in Fig. 38.27, we show a series of Stark-broadened satellite line profiles computed for increasing values of the electron density. The calculation involves all the transitions between the He-like double-excited $2\ell 2\ell'$ states, the relative distribution population assumed to be in local thermodynamic equilibrium (LTE), and the single-excited $1s2\ell$ states. The Stark broadening is treated by the Smith-Hopper relaxation theory with the static ion approximation.[10] The relative distribution of population among doubly excited states was taken to be in LTE. As the density increases, the line shape loses the detailed structure that reflects the set of transitions involved in its calculation and turns into a rather broad and smooth line profile. Yet, at higher densities, the features of the shape still resemble the broad characteristics of the profile at low density (see Fig. 38.27). The fitting of the spectral feature associated with the Ly_α line and its related satellite emission is done using an intensity model that combines the calculated line profiles of satellite and resonance transitions. Opacity broadening is simulated in each line profile by means of the uniform slab model and is characterized by the optical thickness at line center τ_{os} (satellite) and τ_{or} (resonance).[10] Doppler and instrumental broadening are also included. Before the experimental spectra are compared with the theoretical calculations, the continuum background, estimated from the spectrum over a broader range, is subtracted from the data. For a given spectrum and value of the electron density N_e, we pick τ_{or} and τ_{os} for the best possible fit to the experimental data; this is done automatically by a program that minimizes the sum of the square differences between experimental and theoretical (log intensity) points (Q^2). This procedure is repeated for different values of N_e allowing us to see the changes in Q^2 and the values of τ_{or} and τ_{os} as a function of N_e. We find for each spectrum that there is a range of N_e over which Q^2 has a minimum and the quality of the fit is very good. Next, the ratio of optical thickness τ_{or}/τ_{os}, obtained from Q^2 multiplication, can be checked for consistency with the values computed using kinetic modeling. This ratio minimizes any uncertainty in the assumption of a characteristic geometrical length and is proportional to the ratio of populations in the lower state of each transition (ground-state H-like Ar and first, single-excited state in He-like Ar). Independently, a collisional-radiative kinetic code was also used to compute this ratio.[14] We have, therefore, examined the sensitivity of this ratio to different modeling assumptions such as optically thin, optically thick, LTE, or changes in the number of excited states. For electron densities above 1×10^{24} cm^{-3} this ratio is rather insensitive to modeling details and becomes a function of only N_e and T_e. This is because at these high densities the $n = 2$ level of He-like Ar gradually comes into LTE with the ground state ($n = 1$) of H-like Ar, although, for example, this level is not in LTE with the $n = 2$ level of H-like Ar. Comparison with kinetic calculations also lets us estimate values of the electron temperature T_e. An analysis of the data in Figs. 38.25 and 38.26, based on the above procedure, allows us to infer N_e and T_e. Table 38.II summarizes our findings.

Table 38.II Density and temperature results for the analysis of data in Figs. 38.25 and 38.26. Time is measured with respect to the peak of the laser pulse (1×10^{24} cm^{-3} ~ 4 g/cm^3)

Figure Spectrum	Time Interval (ps)	Electron Density (cm^{-3})	Temperature (eV)
1, (a)	109-171	4.0-6.0 $\times$ 10^{24}	600-900
1, (b)	171-233	4.0-6.0 $\times$ 10^{24}	600-900
1, (c)	202-264	4.0-7.0 $\times$ 10^{24}	600-800
1, (d)	233-295	6.0-8.0 $\times$ 10^{24}	500-600
1, (e)	295-357	2.5-6.0 $\times$ 10^{24}	450-600
1, (f)	357-419	2.5-4.0 $\times$ 10^{24}	450-600
2, (a)	312-375	5.0-7.0 $\times$ 10^{24}	600-900
2, (b)	348-405	3.0-6.0 $\times$ 10^{24}	600-800
2, (c)	375-427	6.0-8.0 $\times$ 10^{24}	500-800

E5096

A similar analysis of the spectral feature associated with the He_α line and its Li-like satellite transitions was performed and provides consistent results. An example of the level of agreement between the theoretical fits and the experimental line profiles of both the He_α (3100-3170 eV) and Ly_α (3260-3340 eV) spectral features is illustrated in Fig. 38.28. As can be seen for this particular spectrum, the best fit to both features corresponds to that computed for an electron density of 5×10^{24} cm^{-3}. The continuum background level is also shown. We estimate that effects of temperature and density gradients can introduce uncertainties of less than 50% in our density inferences.[15]

It is important to note that the values of τ_{or} (5-20), deduced in the fitting procedure, are significantly smaller than those required to fit the spectra from previous experiments.[10,11] Before stagnation we find $\tau_{or} > \tau_{os}$, while at, and after, stagnation $\tau_{or} \lesssim \tau_{os}$. One-dimensional hydrodynamic simulations of these experiments indicate that close to stagnation a central region of about 25% of the Ar mass is sufficiently hot to populate the K-shell ions, while the remaining Ar has a temperature in the range 200 eV to 600 eV.[15,16] Ionization balance calculations performed in this temperature range for densities greater than 4 g/cm^3 indicate that the C-, B-, Be-, and Li-like ions share almost all the population and that the population of excited states becomes comparable to, or even exceeds, that for the ground states.[17] These results support the finding of a low opacity effect on resonant transitions and increases the likelihood of opacity effects on satellite transitions.

The analysis of the time-integrated, x-ray pinhole (2 keV to 4 keV), images of the compressed core, showing a spherically imploded Ar

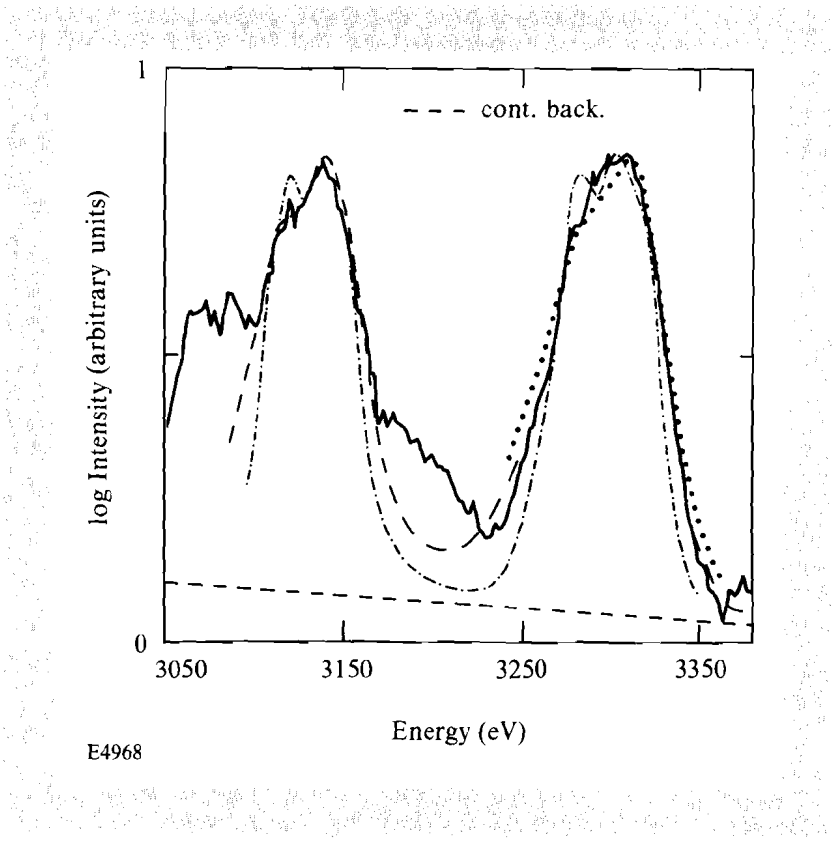

Fig. 38.28
An example of the fittings obtained. This case corresponds to spectrum (b) in Fig. 38.25. Experimental spectrum (——); fitting (— — —). $N_e = 1 \times 10^{24}$ (— · — · —); 5×10^{24} (— — —); and 8×10^{24} (• • • • •) in cm^{-3}.

plasma of 35-μm diameter, is also in reasonable agreement with our spectroscopic analysis. Assuming mass conservation, this would indicate average mass densities of 20 to 40 g/cm^3.

In conclusion, the electron densities recorded here are the largest observed directly through spectroscopic means. Furthermore, the low opacity of the resonance lines, which is consistent with our modeling, implies the existence of radiation "windows" in very dense, hot plasmas. Since the spatial extent of the excited-state orbitals at these densities is comparable to the average interatomic spacing, the onset of the blue satellite features may indicate the initiation of a plasma-solid phase transition.[18] However, additional analysis is required to verify this speculation.

ACKNOWLEDGMENT

This work was supported by the U.S. Department of Energy Office of Inertial Fusion under agreement No. DE-FC03-85DP40200 and by the Laser Fusion Feasibility Project at the Laboratory for Laser Energetics, which has the following sponsors: Empire State Electric Energy Research Corporation, New York State Energy Research and Development Authority, Ontario Hydro, and the University of Rochester. Such support does not imply endorsement of the content by any of the above parties.

REFERENCES

1. S. Skupsky and S. Kacenjar, *J. Appl. Phys.* **52**, 2608 (1981).
2. E. G. Gamalii, S. Yu. Gus'Kov, O. N. Krokhin, and V. B. Rozanov, *JETP Lett.* **21**, 70 (1975).
3. B. Yaakobi *et al.*, *Phys. Rev. Lett.* **39**, 1526 (1977).
4. K. B. Mitchell *et al.*, *Phys. Rev. Lett.* **42**, 232 (1979).
5. J. M. Auerbach *et al.*, *Phys. Rev. Lett.* **44**, 1672 (1980).
6. A. Hauer *et al.*, *Phys. Rev. Lett.* **45**, 1495 (1980).
7. C. F. Hooper, D. P. Kilcrease, R. C. Mancini, L. A. Woltz, D. K. Bradley, P. A. Jaanimagi, and M. C. Richardson, *Phys. Rev. Lett.* (to be published).
8. LLE Review **33**, 1 (1987).
9. B. L. Henke and P. A. Jaanimagi, *Rev. Sci. Instrum.* **56**, 1537 (1985).
10. N. D. Delamater, C. F. Hooper, Jr., R. F. Joyce, L. A. Woltz, N. M. Ceglio, R. L. Kauffman, R. W. Lee, and M. C. Richardson, *Phys. Rev. A* **31**, 2460 (1985).
11. N. D. Delamater, C. F. Hooper, Jr., M. C. Richardson, P. Jaanimagi, R. L. Kauffman, J. Scofield, L. A. Woltz, and T. Garber, *Phys. Rev. A* (in press).
12. C. F. Hooper, Jr., R. C. Mancini, D. P. Kilcrease, L. A. Woltz, M. C. Richardson, D. K. Bradley, and P. A. Jaanimagi, *SPIE* **913**, 129 (1988).
13. R. L. Kauffman (private communication).
14. L. A. Woltz and C. F. Hooper, Jr., *Phys. Rev. A.* **38**, 4766 (1988).
15. R. C. Mancini and C. F. Hooper, Jr., *J. Phys. D* **21**, 1099 (1988).
16. J. Delettrez (private communication).
17. Y. T. Lee, *J. Quant. Spectros. & Radiat. Transfer* **38**, 131 (1987).
18. S. M. Younger, A. K. Harrison, K. Fujima, and D. Griswold, *Phys. Rev. Lett.* **61**, 962 (1988).